
Incorporating Symmetry into Deep Dynamics Models for Improved Generalization

Rui Wang^{*1} Robin Walters^{*2} Rose Yu¹

Abstract

Training machine learning models that can learn complex spatiotemporal dynamics and generalize under distributional shift is a fundamental challenge. The symmetries in a physical system play a unique role in characterizing unchanged features under transformation. We propose a systematic approach to improve generalization in spatiotemporal models by incorporating symmetries into deep neural networks. Our general framework to design equivariant convolutional models employs (1) convolution with equivariant kernels, (2) conjugation by averaging operators in order to force equivariance, (3) and a naturally equivariant generalization of convolution called group correlation. Our framework is both theoretically and experimentally robust to distributional shift by a symmetry group and enjoys favorable sample complexity. We demonstrate the advantage of our approach on a variety of physical dynamics including turbulence and diffusion systems. This is the first time that equivariant CNNs have been used to forecast physical dynamics.

1. Introduction

Modeling dynamical systems in order to forecast the future is of critical importance in fields as diverse as cosmology, economics, and neuroscience (Strogatz, 2018; Izhikevich, 2007; Wainwright & Ellis, 2005; Day, 1994). Many dynamical systems are described by systems of non-linear differential equations which do not have well understood theoretical properties. They cannot be solved analytically and are difficult to simulate numerically due to high sensitivity to initial conditions which leads to instabilities in computational methods.

^{*}Equal contribution ¹Khoury College of Computer Sciences, Northeastern University, Boston, MA ²Department of Mathematics, Northeastern University, Boston, MA. Correspondence to: Rui Wang <wang.rui4@husky.neu.edu>, Robin Walters <r.walters@northeastern.edu>.

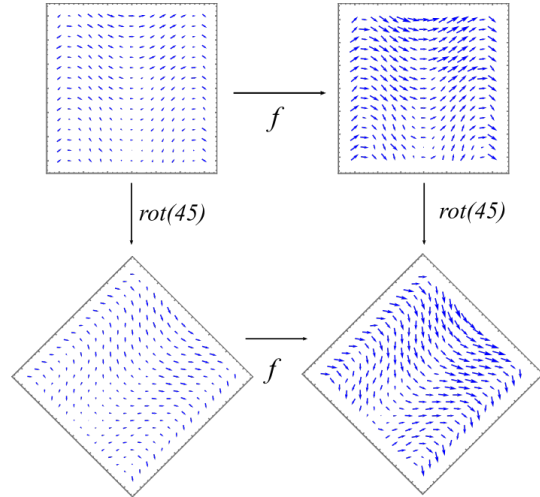


Figure 1. Illustration of equivariance of e.g. $f(x) = 2x$ with respect to $T = \text{rot}(\pi/4)$.

Recently, there has been much work applying deep learning to solve differential equations (Tompson et al., 2017; Chen et al., 2018) or to identify unknown dynamics (Downey et al., 2017; Wang et al., 2019b). However, current approaches struggle with generalization. Given test data with parameters shifted relative to their training data, the accuracy of these models decays rapidly. For example, models trained on data from a certain physical scale fail to generalize to test data from a larger physical scale.

The deep connection between physical dynamics and symmetry transformations suggests it is very natural to incorporate symmetries into a forecasting model to improve generalization. In physics, Noether’s Law gives a correspondence between conserved quantities and groups of symmetries. For example, the translational symmetry corresponds to conservation of momentum. By building a neural network which is inherently translation-equivariant, we thus make conservation of momentum more likely and consequently make the model’s prediction more robust.

Mathematically speaking, a function f is called equivariant if a transformation T of its input x corresponds to the same transformation of its output

$$f(Tx) = Tf(x).$$

See Figure 1 for an illustration. In the setting of forecasting, f approximates the underlying dynamical system. The set of valid transformations T is called the symmetry group of the system.

In this paper, we develop a systematic framework to incorporate symmetries into deep models for learning dynamics. By designing a model that is inherently equivariant to transformations of its input, we can guarantee that our model generalizes automatically across these transformations, making it robust to distributional shift. We design various techniques to enforce (1) translational symmetries, (2) rotational symmetries, (3) uniform motion, and (4) scale equivariance.

Specifically, for rotational symmetries, we leverage the key insight that the input, output and hidden layers of the network are all acted upon by the symmetry group and thus should be treated as representations of the symmetry group. Hence entries of the convolution kernel should not just be scalars but linear transformations between representations. In the case of a uniform motion, also called a Galilean transformation, we design a network in which convolutions are conjugated by averaging operations. For scale equivariance, we replace the convolution operation with group correlation over the group G generated by translations *and* rescalings.

Research into equivariant neural networks has mostly been applied to tasks such as image classification (Kondor & Trivedi, 2018; Weiler et al., 2018; Weiler & Cesa, 2019). In those applications, some layers of the network are equivariant, but the full network is invariant (trivially equivariant). In contrast, we design equivariant networks in a completely different context, that of a time series representing a physical process. Moreover, since we consider transformations of both the input and output, they are designed to be fully equivariant. To the best of our knowledge, this is the first time equivariant convolutional models have been applied to forecasting physical dynamics. Our contributions include:

- We study the problem of improving the generalization capability of deep learning models for learning physical dynamics.
- We develop a systematic framework to incorporate various symmetries, including uniform motion, rotation and scaling, into convolutional neural networks.
- We provide theoretical guarantees for the equivariance properties of our design based on representation theory.
- When evaluated on heat diffusion and turbulence prediction, our framework achieves significant improvement on generalization of both predictions and physical consistency.

2. Mathematical Preliminaries

We begin with a discussion of the mathematics underlying symmetry, called representation theory, and how it can be used to study solutions of differential equations.

2.1. Symmetry groups and Equivariant Functions

Formal discussion of symmetry relies on the concept of an abstract symmetry group. We give a brief overview. For any omitted formal definitions see Appendix A.1, or for a more complete introduction to the topic see Lang (2002).

A **group of symmetries** or simply **group** consists of a set G together with a composition map $\circ: G \times G \rightarrow G$. The composition map is required to be associative and have an identity $1 \in G$. Most importantly, composition with any element of G is required to be invertible.

Example 1. Let $G = GL_2(\mathbb{R})$ be the set of 2x2 invertible real matrices. The set is closed under inversion and matrix multiplication gives a well-defined composition.

Example 2. Let $G = D_3 = \{1, r, r^2, s, rs, r^2s\}$ where r is rotation by $2\pi/3$ and s is reflection over the y -axis. This is the group of symmetries of an equilateral triangle pointing along the y -axis, see Figure 2.

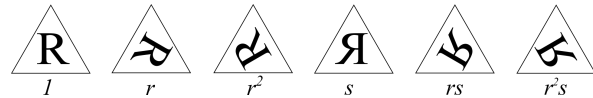


Figure 2. Illustration of D_3 acting on a triangle with the letter “R”.

Groups are abstract objects, but they become concrete when we let them act. A group G has an **action** on a set S if there is an action map $\cdot: G \times S \rightarrow S$ which is compatible with the composition law. We say further that S is a **G -representation** if the set S is a vector space and the group acts on S by linear transformations.

Example 3. The group D_3 acts on S the set of points in an equilateral triangle as in Figure 2. The vector space \mathbb{R}^2 is both a D_3 -representation and a $GL_2(\mathbb{R})$ -representation.

The language of groups and actions allows us to say formally what we mean by invariance and equivariance.

Definition 1 (invariant, equivariant). Let $f: X \rightarrow Y$ be a function and G be a group.

1. Assume G acts on X . The function f is G -invariant if $f(gx) = f(x)$ for all $x \in X$ and $g \in G$.
2. Assume G acts on X and Y . The function f is G -equivariant if $f(gx) = gf(x)$ for all $x \in X$ and $g \in G$.

We can combine and decompose representations in different ways. Given two G -representations V and W , we can create

a new representation, the **direct sum** $V \oplus W$ with action $g \cdot (v, w) = (gv, gw)$. Similarly, the **tensor product** $V \otimes W$ is a G -representation with action $g \cdot v \otimes w = (gv) \otimes (gw)$.

If a G -representation V contains a subspace W which is preserved by the action of G , we call it a **subrepresentation**. An **irreducible representation** V has only 0 and itself as subrepresentations.

Irreducible representations are the ‘‘prime’’ building blocks of representations. A **compact Lie group** is one which is closed and bounded. The rotation group $SO(2, \mathbb{R})$ is compact, but the group $(\mathbb{R}, +)$ is not. The following theorem vastly simplifies our understanding of possible representations of compact Lie groups (see e.g. Knapp (2002)).

Theorem 1 (Weyl’s Complete Reducibility Theorem). *Let G be a compact real Lie group. Every finite-dimensional representation of V is a direct sum of irreducible representations $V = \oplus_i V_i$.*

2.2. Physical Dynamical Systems

We describe the two physical dynamical systems which are the primary examples in this paper.

2D Heat Equation. Let $H(t, x, y)$ be a scalar field representing temperature. Then H satisfies

$$\frac{\partial H}{\partial t} = \alpha \Delta H. \quad (\mathcal{D}_{\text{heat}})$$

Here $\Delta = \partial_x^2 + \partial_y^2$ is the two-dimensional Laplacian and $\alpha \in \mathbb{R}_{>0}$ is the diffusivity.

2D Navier-Stokes (NS) Equations. Let $w(t, x, y)$ be a vector velocity field of a flow. The field w has two components (u, v) , velocities along x and y directions. The governing equations for this physical system are the continuity equation, momentum equation and temperature equation,

$$\begin{aligned} \nabla \cdot w &= 0 \\ \frac{\partial w}{\partial t} &= -(w \cdot \nabla)w - \frac{1}{\rho_0} \nabla p + \nu \nabla^2 w + f \\ \frac{\partial H}{\partial t} &= \kappa \Delta H - (w \cdot \nabla)H \end{aligned} \quad (\mathcal{D}_{\text{NS}})$$

where p and H are pressure and temperature respectively, κ is the coefficient of heat conductivity, ρ_0 is initial density, α is the coefficient of thermal expansion, ν is the kinematic viscosity, and f the body force that is due to gravity. Unlike the heat equations, the advection term $(w \cdot \nabla)w$ above makes this system highly non-linear.

2.3. Symmetries of Differential Equations

By classifying the symmetries of a system of differential equations, the task of finding solutions is made far simpler, since the space of solutions will exhibit those same

symmetries. Let G be a group equipped with an action on 2-dimensional space $X = \mathbb{R}^2$ and 3-dimensional spacetime $\hat{X} = \mathbb{R}^3$. Let $V = \mathbb{R}^d$ be a G -representation. Denote the set of all V -fields on \hat{X} as

$$\hat{\mathcal{F}}_V = \{w : \hat{X} \rightarrow V : w \text{ smooth}\}. \quad (1)$$

Define \mathcal{F}_V similarly to be V -fields on X . Then G has an induced action on $\hat{\mathcal{F}}_V$ by $(gw)(x, t) = g(w(g^{-1}x, g^{-1}t))$ and on \mathcal{F}_V analogously.

Consider a system of (not necessarily linear) differential operators $\mathcal{D} = \{P_1, \dots, P_r\}$ acting on $\hat{\mathcal{F}}_V$. The solution space is then $\text{Sol}(\mathcal{D}) = \{\varphi \in \hat{\mathcal{F}}_V : P_i(\varphi) = 0 \text{ for all } i\}$.

Definition 2 (symmetry of differential system). We say that G is a *symmetry group of the system \mathcal{D}* if the action of G preserves $\text{Sol}(\mathcal{D}) \subseteq \hat{\mathcal{F}}_V$. That is, if φ is a solution of \mathcal{D} , then for all $g \in G$, $g(\varphi)$ is as well.

Symmetries of Heat and NS Equations. Table 1 shows the symmetries of Heat and Navier-Stokes Equations we study in this paper. The full list of symmetries can be found in appendix A.7.

Table 1. Symmetries of Heat Equation and Navier-Stoke Equation

Symmetries	Heat Equ.	NS Equ.	Params
Space translation	$H(\mathbf{x} - \mathbf{v}, t)$	$w(\mathbf{x} - \mathbf{v}, t)$	$\mathbf{v} \in \mathbb{R}^2$
Time translation	$H(\mathbf{x}, t - \tau)$	$w(\mathbf{x}, t - \tau)$	$\tau \in \mathbb{R}$
Uniform Motion	$\eta H(\mathbf{x} - 2\mathbf{v}t, t)$	$w(\mathbf{x}, t) + \mathbf{c}$	$\mathbf{c} \in \mathbb{R}^2$
Reflect/rotation	$H(R\mathbf{x}, t)$	$Rw(R^{-1}\mathbf{x}, t)$	$R \in O(2)$
Scaling	$H(\lambda\mathbf{x}, \lambda^2 t)$	$\lambda w(\lambda\mathbf{x}, \lambda^2 t)$	$\lambda \in \mathbb{R}_{>0}$

2.4. Equivariance of the Forward Prediction

In order to forecast the evolution of a system \mathcal{D} , we need to model the forward prediction function f . Fix a time t and timestep τ . To simplify notation, we assume units in which $\tau = 1$. Let $w \in \text{Sol}(\mathcal{D})$. Then our input to f is a collection of k snapshots at times $t - k, \dots, t - 1$ denoted $w_{t-i} \in \mathcal{F}_d$. The prediction function $f : \mathcal{F}_d^k \rightarrow \mathcal{F}_d$ is defined $f(w_{t-k}, \dots, w_{t-1}) = w_t$. It predicts the solution at a time t based on the solution in the past.

Let G be a symmetry group of \mathcal{D} . Then for $g \in G$, $g(w)$ is also a solution of \mathcal{D} . Thus $f(gw_{t-k}, \dots, gw_{t-1}) = gw_t$. Consequently, the forward prediction function is equivariant with respect to the symmetry group of the system \mathcal{D} .

3. Methodology

We summarize the model design requirement for networks to be equivariant. Then we describe our approaches to incorporate various symmetries into these models.

3.1. Equivariant Networks

The key to building equivariant networks is that the composition of equivariant functions is equivariant. Hence, if the maps between layers of a neural network are equivariant, then the whole network will be equivariant. Note that both the linear maps and activation functions must be equivariant.

A very important consequence of this principle is that the hidden layers must also carry a G -action. Thus, the hidden layers are not collections of scalar channels, but G -representations. If G is compact, then by Theorem 1, we may simplify by decomposing each hidden layer into a direct sum of irreducible representations.

Equivariant Convolutions. Consider a convolutional layer $\mathcal{F}_{\mathbb{R}^{d_{\text{in}}}} \rightarrow \mathcal{F}_{\mathbb{R}^{d_{\text{out}}}}$ with kernel K from a $\mathbb{R}^{d_{\text{in}}}$ -field to a $\mathbb{R}^{d_{\text{out}}}$ -field. Assume that $\mathbb{R}^{d_{\text{in}}}$ and $\mathbb{R}^{d_{\text{out}}}$ are G -representations with action maps ρ_{in} and ρ_{out} respectively. It is proved in Weiler & Cesa (2019) that the network is G -equivariant if and only if

$$K(gv) = \rho_{\text{out}}^{-1}(g)K(v)\rho_{\text{in}}(g) \quad \text{for all } g \in G. \quad (2)$$

Skip Connections. The ResNet and U-net architectures contain skip connections. Define $f^{(ij)}$ as the functional mapping between layer i and layer j . The following proposition proves that adding skip connections to a network does not affect its equivariance with respect to linear actions.

Proposition 2. *Let the layer $V^{(i)}$ be a G -representations for $0 \leq i \leq n$. Let $f^{(ij)}: V^{(i)} \rightarrow V^{(j)}$ be G -equivariant for $i < j$. Define recursively $\mathbf{x}^{(j)} = \sum_{0 \leq i < j} f^{(ij)}(\mathbf{x}^{(i)})$. Then $\mathbf{x}^{(n)} = f(\mathbf{x}^{(0)})$ is G -equivariant.*

Proof. Assume $\mathbf{x}^{(i)}$ is an equivariant function of $\mathbf{x}^{(0)}$ for $i < j$. Then by equivariance of $f^{(ij)}$ and by linearity of the G -action,

$$\sum_{0 \leq i < j} f^{(ij)}(g\mathbf{x}^{(i)}) = \sum_{0 \leq i < j} gf^{(ij)}(\mathbf{x}^{(i)}) = g\mathbf{x}^{(j)},$$

for $g \in G$. By induction, $\mathbf{x}^{(n)} = f(\mathbf{x}^{(0)})$ is equivariant with respect to G . \square

Both ResNet and U-net may be modeled as in Proposition 2 with some convolutional and activation components $f^{(i,i+1)}$ and some skip connections $f^{(ij)} = I$ with $j-i \geq 2$. Since I is equivariant for any G , we thus have:

Corollary 3. *If the layers of ResNet or U-net are G -representations and the convolutional mappings and activation functions are G -equivariant, then the entire network is G -equivariant.* \square

Corollary 3 allows us to build equivariant convolutional networks for rotational and scaling transformations, which are linear actions.

3.2. Time and Space Translation Equivariance

Convolutional neural networks (CNNs) are time translation-equivariant as long as we predict in an autoregressive manner. Convolutional layers are also naturally space translation-equivariant (if cropping is ignored). Any activation function which acts identically pixel-by-pixel is equivariant. Both ResNet and U-net are time and space translation equivariant due to the following proposition proved in Appendix A.4.

Proposition 4. *Adding skip connections to a translation-equivariant network preserves translation-equivariance.*

3.3. Rotational Equivariance

To incorporate rotational symmetries, we model the dynamics of f using G -equivariant convolutions and activations where $G = SO(2)$. The irreducible representations of $SO(2)$ are the trivial one-dimensional representation ρ_0 and

$$\begin{aligned} \rho_n : G &\mapsto GL(\mathbb{R}^2), \quad n \in \mathbb{Z}_{\neq 0} \\ g &\mapsto \begin{pmatrix} \cos(n\theta) & -\sin(n\theta) \\ \sin(n\theta) & \cos(n\theta) \end{pmatrix}. \end{aligned} \quad (3)$$

In a ρ_n -vector field a rotation of the base space by angle θ corresponds to a rotation $n\theta$ of the vectors in the field. Using this notation, the input to our model is k ρ_1 -vector fields and the output is a single ρ_1 -vector field.

Consider a hidden layer which is a ρ -field for some finite-dimensional G -representation ρ . Since the group $SO(2)$ is compact, by Theorem 1, ρ can be decomposed as a direct sum of irreducible $SO(2)$ -representations $\bigoplus_i \rho_{n_i}$. It thus suffices to consider convolutions for all n, m from a ρ_n -field to ρ_m -field which satisfy (2). These are classified in Weiler & Cesa (2019).

We give some examples of convolutional kernels which are rotationally equivariant in the sense of (2). A convolution $K : \mathcal{F}_{\rho_0} \rightarrow \mathcal{F}_{\rho_0}$ has $K(gv) = K(v)$. A convolutional kernel $\mathcal{F}(\rho_1^{d_{\text{in}}}) \rightarrow \mathcal{F}(\rho_1^{d_{\text{out}}})$, on the other hand, would have shape $(d_{\text{out}}, d_{\text{in}}, s, s, 2, 2)$. That is, since ρ_1 is two-dimensional, the entries of the $s \times s$ kernel are not scalars, but 2×2 matrices, as in Fig. 3.

In practice, we use $G = C_n$ instead of $G = SO(2)$ as for large enough n the difference is practically indistinguishable due to space discretization. The activation function must be rotationally symmetric. This means an activation function $\sigma: \mathbb{R}^2 \rightarrow \mathbb{R}^2$ must be a non-linear magnitude-rescaling $\sigma(v) = r(|v|)v/|v|$ where $r: \mathbb{R}_{\geq 0} \rightarrow \mathbb{R}_{\geq 0}$.

Choice of Hidden Layer Representations. For an equivariant neural network, we must choose not only the dimension of the hidden layers, but which representations of G the hidden layers are. We present a representation theoretic

principle for making this decision. Namely, that the irreducible representation types in the hidden layers should be of the *same type* and in the *same proportion* as those that appear in the input and output. Schur’s lemma (Lang, 2002) implies that linear G -maps between irreducible representations of different types are 0. This implies there should not be a map from a layer which has a given type of irreducible representation to one that does not. For example, in order to model an $SO(2)$ -equivariant function $\rho_1 \oplus \rho_2 \rightarrow \rho_1 \oplus \rho_2$, the hidden layers should have the form $\rho_1^d \oplus \rho_2^d$.

In our case, we are modeling a function $\mathcal{F}_{\rho_1}^k \rightarrow \mathcal{F}_{\rho_1}$. In order to apply our principle, we must decompose \mathcal{F}_{ρ_1} into irreducible representations. After discretizing and bounding space, i.e. replacing \mathbb{R}^2 by $[0, 64]^2$, and approximating $SO(2)$ by C_n , the space \mathcal{F}_{ρ_1} becomes finite-dimensional, and we may decompose it as a direct sum of m copies of the regular representation V of C_n . We thus model our hidden layers as V^d for various d (see Appendix A.2).

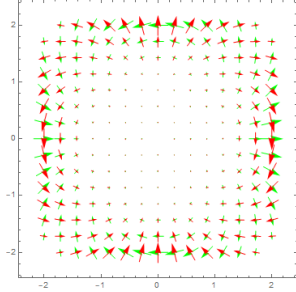


Figure 3. Examples of 2×2 -matrix-valued ρ_1 -rotationally-equivariant kernels. We represent the columns of the matrix as vector fields.

3.4. Uniform Motion Equivariance

Enforcing uniform motion equivariance by requiring the layers of the CNN to be equivariant, however, severely limits the model. As shown in Corollary 8 in appendix, the network would have to be an affine function.

To overcome this limitation, we relax the requirement by conjugating the model with shifted input distribution. For each sliding local block in each convolutional layer, we shift the mean of input tensor to zero and shift the output back after convolution and activation function per sample. In other words, if the input is $\mathcal{P}_{b \times d_{in} \times s \times s}$ and the output is $\mathcal{Q}_{b \times d_{out}} = \mathcal{P} \cdot K$ for one sliding local block, where b is batch size, d is number of channels, s is the kernel size and K is the kernel, then

$$\begin{aligned} \mu_i &= \text{Mean}_{jkl} (\mathcal{P}_{ijkl}); \\ \mathcal{P}_{ijkl} &\mapsto \mathcal{P}_{ijkl} - \mu_i; \\ \mathcal{Q}_{ij} &\mapsto \mathcal{Q}_{ij} + \mu_i. \end{aligned} \quad (4)$$

This will allow the convolution layer to be equivariant with respect to uniform motion. If the input is a vector field, we apply this operation to each element.

For skip connections, it is worth mentioning that the residual function should be *invariant*, not equivariant, to uniform

motion. That is, given a skip connection, $f^{(i,i+2)}$ should be identity function, which is equivariant, then the residual function $f^{(i,i+1)}$ should be invariant. Hence, for the first layer in each residual block, we subtract the mean from the input without adding it back to its output.

3.5. Scale Equivariance

Scale equivariance in dynamics is unique as the physical law dictates the scaling of magnitude, space and time simultaneously. This is very different from scaling in images regarding resolutions (Worrall & Welling, 2019). For example, the Navier-Stokes equations are preserved under a specific scaling ratio of time, space, and velocity given by the transformation

$$\mathbf{w}(x, t) \mapsto \lambda \mathbf{w}(\lambda x, \lambda^2 t), \quad (5)$$

where $\lambda \in \mathbb{R}_{>0}$. There are two approaches for scale equivariance, depending on whether we tie the physical scale with the resolution of the data.

Resolution Independent Scaling. We fix the resolution and scale the magnitude of the input by varying the discretization step size. Given an input $\mathbf{w} \in \mathcal{F}_{\mathbb{R}^2}^k$ with step size $\Delta_x(\mathbf{w})$ and $\Delta_t(\mathbf{w})$ can be scaled $\mathbf{w}' = T_{\lambda}^{sc}(\mathbf{w}) = \lambda \mathbf{w}$ by scaling the magnitude of vector alone, provided the discretization constants are now assumed to be $\Delta_x(\mathbf{w}') = 1/\lambda \Delta_x(\mathbf{w})$ and $\Delta_t(\mathbf{w}') = 1/\lambda^2 \Delta_t(\mathbf{w})$. The model thus does not have a fixed physical scale for its inputs, but it does assume the input’s discretization constants lie on some fixed parabolic curve $\Delta_x^2 = \Delta_t \lambda$ where λ is an arbitrary constant which remains fixed across training and testing.

To obtain scale equivariance, we scale the standard deviation of input tensor to zero and scale the output back after convolution and activation function per sample. Specifically, using the same notations in section 3.4,

$$\begin{aligned} \sigma_i &= \text{Std}_{jkl} (\mathcal{P}_{ijkl}); \\ \mathcal{P}_{ijkl} &\mapsto \mathcal{P}_{ijkl} / \sigma_i; \\ \mathcal{Q}_{ij} &\mapsto \mathcal{Q}_{ij} \cdot \sigma_i. \end{aligned} \quad (6)$$

Resolution Dependent Scaling. If the physical scale of the data is fixed, then scaling the space and time domain corresponds to a change in resolution and time step size. For images, downscaling introduces information loss whereas for physical systems, it is merely an artifact of discretization and not inherent to the physical scaling laws. In particular, it follows from the physical scaling law that our model should be equivariant to up and down scaling and by any positive real number factor.

We replace the convolution layers with group correlation layers over the group $G = (\mathbb{R}_{>0}, \cdot) \times (\mathbb{R}^2, +)$ of scaling and translations. In convolution, we translate a kernel K across

an input p as such $v(p) = \sum_{q \in \mathbb{Z}^2} w(p+q)K(q)$. The G -correlation upgrades this operation by both translating *and* scaling the kernel relative to the input:

$$v(p) = \sum_{\lambda \in \mathbb{Z}_{>0}, q \in \mathbb{Z}^2} (T_\lambda w)(p+q)(T_\lambda K)(q),$$

the transformation T_λ coming from (5).

Our model is equivariant to both up and down scaling and by any $\lambda \in \mathbb{R}_{>0}$, not only powers of two, as in Worrall & Welling (2019). In addition, the scaling symmetry of (5) demands that we scale *anisotropically*, i.e. differently across time and space. To account for this difference, instead of using conv3D which is computationally expensive in practice, we use conv2D on spatial dimensions and a dense network on the time dimension. Our implementation also uses the antialiased rescaling as a composite of Gaussian blur and dilation. Doing so allows the use of the dilation feature of conv2D which accelerates computation.

4. Related work

Equivariance and Invariance. Developing neural nets that preserve symmetries, including rotation, scaling, translation, reflection, etc., has been a fundamental task in image recognition (Worrall & Welling, 2019; Cohen et al., 2019; Weiler & Cesa, 2019; Cohen & Welling, 2016a; Chidester et al., 2018; Lenc & Vedaldi, 2015; Kondor & Trivedi, 2018; Bao & Song, 2019; Worrall et al., 2017; Cohen & Welling, 2016b; Weiler et al., 2018; Dieleman et al., 2016). But these models have never been applied to forecasting physical dynamics. Jaiswal et al. (2019); Moyer et al. (2018) proposed approaches to find the representations of data that are invariant to changes in specified factors, which is different from our physical symmetries. Ling et al. (2017); Fang et al. (2018) studied tensor invariant neural networks to learn the Reynolds stress tensor while preserving Galilean invariance, and Mattheakis et al. (2019) embedded even/odd symmetry of a function and energy conservation into neural networks to solve differential equations. But these two papers are limited to fully connected neural networks.

Physics-informed Deep Learning. Deep learning models have been used a lot to model physical dynamics. For example, Wang et al. (2019a) unified the CFD technique and U-net to generate predictions with higher accuracy and better physical consistency. Kim & Lee (2020) studied unsupervised generative modeling of turbulent flows but the model is not able to make real time future predictions given the historic data. Raissi et al. (2017; 2019) applied deep neural networks to solve PDEs automatically but these approaches require explicitly inputs of boundary conditions during inference, which are generally not available in real-time. Mohan et al. (2019) proposed a purely data-driven

DL model for turbulence, but the model lacks physical constraints and interpretability. Wu et al. (2019) and Beucler et al. (2019) introduced statistical and physical constraints in the loss function to regularize the predictions of the model. However, their studies only focused on spatial modeling without temporal dynamics.

Video Prediction. Our work is also related to future video prediction. Conditioning on the observed frames, video prediction models are trained to predict future frames, e.g., (Mathieu et al., 2015; Finn et al., 2016; Xue et al., 2016; Villegas et al., 2017; Finn et al., 2016). Many of these models are trained on natural videos with complex noisy data from unknown physical processes. Therefore, it is difficult to explicitly incorporate physical principles into these models. Our work is substantially different because we do not attempt to predict object or camera motions.

5. Experiments

5.1. Datasets

We test our models on two dynamical systems: Heat Equation and Rayleigh-Bénard convection.

The Heat Equation plays a major role in studying heat transfer, Brownian motion and particle diffusion. We simulate the heat equation at various initial conditions and thermal diffusivity using the finite difference method and generate $6k$ scalar temperature fields. Figure 4 shows a heat diffusion process where the temperature inside the circle is higher than the outside and the thermal diffusivity is 4.

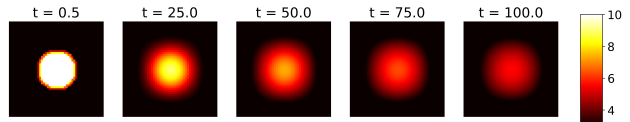


Figure 4. Five snapshots in heat diffusion dynamics. The spatial resolution is 50×50 pixels.

Rayleigh-Bénard convection is a horizontal layer of fluid heated from below, which is a major feature of the El Niño dynamics. The dataset comes from two dimensional turbulent flow simulated using the Lattice Boltzmann Method (Chirila, 2018) with Rayleigh number = 2.5×10^8 . We divided each 1792×256 image into 7 square sub-regions of size 256×256 , then downsample them into 64×64 pixels sized images. We use a sliding window approach to generate 10k samples of sequences of velocity fields. Figure 5 shows a snapshot in our RBC flow dataset.

Data Transformation. We generate the following test sets to test the models’ generalization ability.

- *Uniform motion (UM)*: transformed test sets by adding random vectors drawn from $U(-1, 1)$.

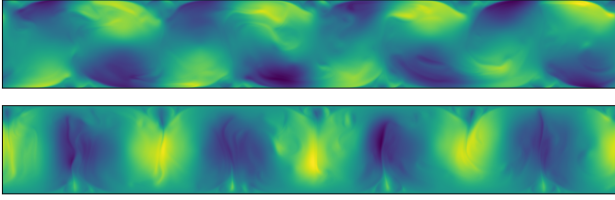


Figure 5. A snapshot of the Rayleigh-Bénard convection flow, the velocity fields along x direction (top) and y direction (bottom) (Chirila, 2018). The spatial resolution is 1792×256 pixels.

- *Magnitude (Mag)*: transformed test sets by multiplying random values sampled from $U(0, 2)$.
- *Rotation (Rot)*: transformed test sets have original test samples randomly rotated by the multiples of $\frac{\pi}{12}$.
- *Scale*: transformed test sets by scaling each sample λ sampled from $U(\frac{1}{5}, 2)$.

Experimental Setup. We implemented two convolutional architectures, ResNet and U-net, equipped with four different symmetries, which we name as Equ-ResNet (U-net). All models predict autoregressively using a loss function that accumulates the forecasting errors over 10 steps. We use 60%-20%-20% training-validation-test split and use the validation set for hyper-parameters tuning based on the average error of predictions. The hyper-parameters tuning range can be found in Table 5 in the appendix A.8. We evaluate models based on the averages and standard deviations of prediction errors over five runs.

5.2. Evaluation Metric

Root Mean Square Error. We calculate the Root Mean Square Error (RMSE) of 10 steps ahead predictions from the ground truth over all pixels.

Thermal Energy Loss. For heat diffusion, due to the law of energy conservation, the sum of each temperature field should be consistent over the entire heat diffusion process. We evaluate the physical characteristics of the predictions using the L1 loss of the thermal energy.

Energy Spectrum Error. For turbulence, we calculate the Energy Spectrum $E(k)$ for the velocity fields, which is related to the mean turbulence kinetic energy as $\int_0^\infty E(k)dk = \frac{(\overline{u'})^2 + (\overline{v'})^2}{2}$, where the k is the wavenumber. The spectrum shows how much kinetic energy is contained in eddies with wavenumber k . We also report the RMSE regarding the Log of Energy Spectrum.

5.3. Results

Since the heat equation is much simpler than the NS equations, a shallow CNN suffices to forecast the heat diffusion process. We evaluate our models on all symmetries except

for uniform motion of the heat equations because it does not fit in our current framework. Table 2 shows the prediction RMSE and thermal energy loss of the CNNs and three Equ-CNNs on three transformed test sets. We can see that Equ-CNNs consistently outperform CNNs over the three test sets.

Table 2. The prediction RMSE and thermal energy L1 loss of the CNNs and three Equ-CNNs on three **transformed** test sets. Equ-CNNs outperform the CNNs over all three test sets.

Testsets \ Models	RMSE (Thermal Energy Loss)		
	<i>Mag</i>	<i>Rot</i>	<i>Scale</i>
CNNs	0.103(4696.3)	0.308(1125.6)	0.357(1447.6)
Equ-CNNs	0.028(107.7)	0.153(127.3)	0.045(396.6)

Table 3 shows the RMSE and the energy spectrum error of predictions on the original and four transformed test sets of turbulent flows by the ResNet (Unet) and four Equ-ResNets (Unets). Each column contains the prediction errors by the non-equivariant and equivariant models on each test set. On the original test set, all models have similar RMSE, yet the equivariant ones have lower energy spectrum errors. It demonstrates that incorporating symmetries into convolutional layers preserves the representation powers of CNNs and even improves models' physical consistency.

On the transformed test sets, we can see that ResNet (Unet) fails, while Equ-ResNets (Unets) performs quite well. As we expected, the uniform motion and magnitude equivariant models are perfectly equivariant and performs consistently well on the original and the corresponding transformed test sets. Rotational equivariant models also outperform the non-equivariant ones. We observe that rotational equivariant models have lower accuracy on the rotation transformed test set than on the original test set. This is because the rotational equivariant models are only perfectly rotational equivariant to the multiple of $\frac{\pi}{2}$ due to the nature of the grid.

Figure 6 shows the ground truth and the predicted u velocity fields at time step 1, 5 and 10 by the ResNet and four Equ-ResNets on the four transformed test samples. From left to right, the transformed test samples are the original test samples uniform motion shifted by $(1, -0.5)$, magnitude scaled by 1.5, rotated by 90 degrees and upsampled by 3 respectively. We can see that ResNet performed poorly while the predictions by Equ-ResNets are still quite close to the target.

We want to evaluate models' generalization ability with respect to the extent of distributional shift. We created additional test sets with different scale factors from $\frac{1}{5}$ to

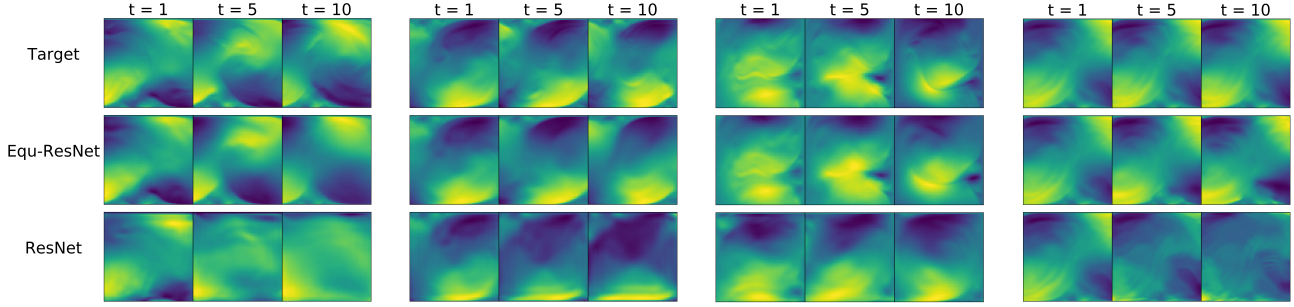


Figure 6. The ground truth and the predicted u velocity fields at time step 1, 5 and 10 by the ResNet and four Equ-ResNets on the four transformed test samples. From left to right, the transformed test samples are the original test samples uniform-motion-shifted by $(1, -0.5)$, magnitude-scaled by 1.5, rotated by 90 degrees and upscaled by 3 respectively. The first row is the target, the second row is Equ-ResNets predictions, and the third row is predictions by ResNet.

Table 3. The RMSE and the energy spectrum errors of the ResNet (Unet) and four Equ-ResNets (Unets) predictions on the original and four transformed test sets of turbulent flows. Each column contains models' prediction errors on each test set.

Testsets \ Models	Root Mean Square Error(10^3)					Energy Spectrum Errors				
	Orig	UM	Mag	Rot	Scale	Orig	UM	Mag	Rot	Scale
ResNet	0.678 ± 0.249	2.940 ± 0.841	4.301 ± 1.275	2.999 ± 0.864	1.964 ± 0.164	0.457 ± 0.190	0.557 ± 0.290	0.259 ± 0.142	1.588 ± 0.424	4.315 ± 2.328
Equ _{UM}	0.710 ± 0.262	0.710 ± 0.262				0.329 ± 0.110	0.329 ± 0.110			
Equ _{Mag}	0.696 ± 0.239		0.676 ± 0.135			0.340 ± 0.088		0.195 ± 0.019		
Equ _{Rot}	0.647 ± 0.262			1.528 ± 0.280		0.309 ± 0.059			0.825 ± 0.052	
Equ _{Scale}	0.702 ± 0.020				0.850 ± 0.085	0.437 ± 0.224				0.676 ± 0.256
U-net	0.646 ± 0.248	2.279 ± 0.828	3.595 ± 1.040	2.274 ± 0.818	1.658 ± 0.173	0.508 ± 0.049	0.349 ± 0.100	0.559 ± 0.050	0.312 ± 0.056	4.250 ± 0.577
Equ _{UM}	0.689 ± 0.263	0.710 ± 0.239				0.228 ± 0.060	0.135 ± 0.056			
Equ _{Mag}	0.673 ± 0.105		0.676 ± 0.135			0.418 ± 0.043		0.347 ± 0.069		
Equ _{Rot}	0.687 ± 0.253			1.528 ± 0.280		0.111 ± 0.019			0.237 ± 0.025	
Equ _{Scale}	0.699 ± 0.134				0.901 ± 0.257	0.451 ± 0.324				0.898 ± 0.298

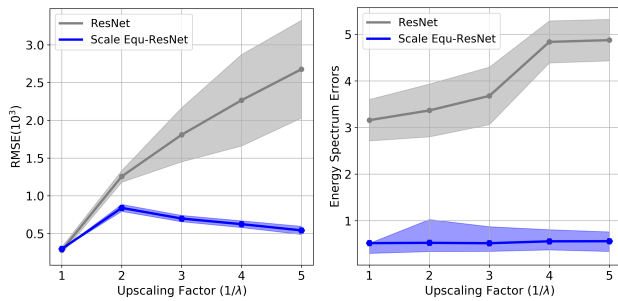


Figure 7. The prediction RMSEs(left) and Spectrum errors(right) of ResNet and Scale Equivariant ResNet on the test sets upscaled by different factors.

1. Figure 7 shows the mean and variance of ResNet and Scale Equ-ResNet prediction RMSEs (left) and Energy Spectrum errors (right) over five runs on the test sets upscaled by different factors. We observed that Scale Equ-ResNet is very robust across various scaling factors while ResNet does not generalize.

6. Discussion and Future work

We develop a systematic framework to improve the generalization of deep sequence models for learning physical dynamics. We incorporate various symmetries by designing equivariant neural networks and demonstrate their superior performance on 2D time series prediction tasks both theoretically and experimentally. Our framework obtains improved physical consistency in the predictions. In the case of transformed test data, our models generalize significantly better than their non-equivariant counterparts. More importantly, all of our equivariant models can be combined and can be extended to 3D cases.

We remark that the group G also acts on the boundary conditions and external forces of a system \mathcal{D} . If these are invariant with respect to the G -action, then the system \mathcal{D} is strictly invariant as in Section 2.3. In practice, these assumptions may be lacking, in which case one must consider a family of solutions with different external forces and boundary conditions to retain equivariance $\cup_{g \in G} \text{Sol}(g\mathcal{D})$. Future work includes speeding up the the scale-equivariant models and incorporating other symmetries into deep learning models.

7. Acknowledgements

This research used resources of the National Energy Research Scientific Computing Center, a DOE Office of Science User Facility supported by the Office of Science of the U.S. Department of Energy under Contract No. DE-AC02-05CH11231. We thank Karthik Kashinath and Mustafa Mustafa for helpful discussions. We also thank Dragos Bogdan Chirila for providing the turbulent flow data.

References

- Bao, E. and Song, L. Equivariant neural networks and equivarification. *arXiv preprint arXiv:1906.07172*, 2019.
- Beucler, T., Pritchard, M., Rasp, S., Gentine, P., Ott, J., and Baldi, P. Enforcing analytic constraints in neural networks emulating physical systems. *arXiv preprint arXiv:1909.00912*, 2019.
- Chen, T. Q., Rubanova, Y., Bettencourt, J., and Duvenaud, D. K. Neural ordinary differential equations. In *Advances in neural information processing systems*, pp. 6571–6583, 2018.
- Chidester, B., Do, M. N., and Ma, J. Rotation equivariance and invariance in convolutional neural networks. *arXiv preprint arXiv:1805.12301*, 2018.
- Chirila, D. B. *Towards lattice Boltzmann models for climate sciences: The GeLB programming language with applications*. PhD thesis, University of Bremen, 2018.
- Cohen, T. S. and Welling, M. Group equivariant convolutional networks. In *International conference on machine learning (ICML)*, pp. 2990–2999, 2016a.
- Cohen, T. S. and Welling, M. Steerable CNNs. *arXiv preprint arXiv:1612.08498*, 2016b.
- Cohen, T. S., Weiler, M., Kicanaoglu, B., and Welling, M. Gauge equivariant convolutional networks and the icosahedral CNN. In *Proceedings of the 36th International Conference on Machine Learning (ICML)*, volume 97, pp. 1321–1330, 2019.
- Day, R. H. Complex economic dynamics-vol. 1: An introduction to dynamical systems and market mechanisms. *MIT Press Books*, 1, 1994.
- Dieleman, S., Fauw, J. D., and Kavukcuoglu, K. Exploiting cyclic symmetry in convolutional neural networks. In *International Conference on Machine Learning (ICML)*, 2016.
- Downey, C., Hefny, A., Boots, B., Gordon, G. J., and Li, B. Predictive state recurrent neural networks. In *Advances in Neural Information Processing Systems*, pp. 6053–6064, 2017.
- Fang, R., Sondak, D., Protopapas, P., and Succi, S. Deep learning for turbulent channel flow. *arXiv preprint arXiv:1812.02241*, 2018.
- Finn, C., Goodfellow, I., and Leine, S. Unsupervised learning for physical interaction through video prediction. In *Advances in neural information processing systems*, pp. 64–72, 2016.
- Izhikevich, E. M. *Dynamical systems in neuroscience*. MIT press, 2007.
- Jaiswal, A., Moyer, D., Steeg, G. V., AbdAlmageed, W., and Natarajan, P. Invariant representations through adversarial forgetting. *arXiv preprint arXiv:1911.04060*, 2019.
- Kim, J. and Lee, C. Deep unsupervised learning of turbulence for inflow generation at various Reynolds numbers. *Journal of Computational Physics*, pp. 109216, 2020.
- Knapp, A. W. *Lie Groups Beyond an Introduction*, volume 140 of *Progress in Mathematics*. Birkhäuser, Boston, 2nd edition, 2002.
- Kondor, R. and Trivedi, S. On the generalization of equivariance and convolution in neural networks to the action of compact groups. In *Proceedings of the 35th International Conference on Machine Learning (ICML)*, volume 80, pp. 2747–2755, 2018.
- Lang, S. *Algebra*. Springer, Berlin, 3rd edition, 2002.
- Lenc, K. and Vedaldi, A. Understanding image representations by measuring their equivariance and equivalence. In *Proceedings of the IEEE conference on computer vision and pattern recognition*, pp. 991–999, 2015.
- Ling, J., Kurzwaskim, A., and Templeton, J. Reynolds averaged turbulence modeling using deep neural networks with embedded invariance. *Journal of Fluid Mechanics*, 2017.
- Mathieu, M., Couprie, C., and LeCun, Y. Deep multi-scale video prediction beyond mean square error. *arXiv preprint arXiv:1511.05440*, 2015.
- Mattheakis, M., Protopapas, P., Sondak, D., Giovanni, M. D., and Kaxiras, E. Physical symmetries embedded in neural networks. *arXiv preprint arXiv:1904.08991*, 2019.
- Mohan, A., Daniel, D., Chertkov, M., and Livescu, D. Compressed convolutional LSTM: An efficient deep learning framework to model high fidelity 3D turbulence. *arXiv preprint arXiv:1903.00033*, 2019.
- Moyer, D., Gao, S., Brekelmans, R., Galstyan, A., and Ver Steeg, G. Invariant representations without adversarial training. In *Advances in Neural Information Processing Systems (NeurIPS)*, pp. 9084–9093, 2018.

- Olver, P. J. *Applications of Lie groups to differential equations*, volume 107. Springer Science & Business Media, 2000.
- Raissi, M., Perdikaris, P., and Karniadakis, G. E. Physics informed deep learning (part I): Data-driven solutions of nonlinear partial differential equations. *arXiv preprint arXiv:1711.10561*, 2017.
- Raissi, M., Perdikaris, P., and Karniadakis, G. E. Physics-informed neural networks: A deep learning framework for solving forward and inverse problems involving nonlinear partial differential equations. *Journal of Computational Physics*, 378:686–707, 2019.
- Strogatz, S. H. *Nonlinear dynamics and chaos: with applications to physics, biology, chemistry, and engineering*. CRC press, 2018.
- Tompson, J., Schlachter, K., Sprechmann, P., and Perlin, K. Accelerating Eulerian fluid simulation with convolutional networks. In *Proceedings of the 34th International Conference on Machine Learning (ICML)*, volume 70, pp. 3424–3433, 2017.
- Villegas, R., Yang, J., Hong, S., Lin, X., and Lee, H. Decomposing motion and content for natural video sequence prediction. 2017.
- Wainwright, J. and Ellis, G. F. R. *Dynamical systems in cosmology*. Cambridge University Press, 2005.
- Wang, R., Kashinath, K., Mustafa, M., Albert, A., and Yu, R. Towards physics-informed deep learning for turbulent flow prediction. *arXiv preprint arXiv:1911.08655*, 2019a.
- Wang, Y., Smola, A., Maddix, D., Gasthaus, J., Foster, D., and Januschowski, T. Deep factors for forecasting. In *Proceedings of the 36th International Conference on Machine Learning (ICML)*, volume 97, pp. 6607–6617, 2019b.
- Weiler, M. and Cesa, G. General E(2)-equivariant steerable CNNs. In *Advances in Neural Information Processing Systems (NeurIPS)*, pp. 14334–14345, 2019.
- Weiler, M., Hamprecht, F. A., and Storath, M. Learning steerable filters for rotation equivariant CNNs. *Computer Vision and Pattern Recognition (CVPR)*, 2018.
- Worrall, D. and Welling, M. Deep scale-spaces: Equivariance over scale. In *Advances in Neural Information Processing Systems (NeurIPS)*, pp. 7364–7376, 2019.
- Worrall, D. E., Garbin, S. J., Turmukhambetov, D., and Brostow, G. J. Harmonic networks: Deep translation and rotation equivariance. In *Proceedings of the IEEE Conference on Computer Vision and Pattern Recognition*, pp. 5028–5037, 2017.
- Wu, J.-L., Kashinath, K., Albert, A., Chirila, D., Prabhat, and Xiao, H. Enforcing statistical constraints in generative adversarial networks for modeling chaotic dynamical systems. *Journal of Computational Physics*, pp. 109209, 2019.
- Xue, T., Wu, J., Bouman, K., and Freeman, B. Visual dynamics: Probabilistic future frame synthesis via cross convolutional networks. In *Advances in neural information processing systems (NeurIPS)*, pp. 91–99, 2016.

A. Appendix

A.1. Formal Definitions of Group Theory

We give here the formal definitions which have been omitted from Section 2.1.

Definition 3 (group). A group of symmetries or simply *group* is a set G together with a binary operation $\circ: G \times G \rightarrow G$ called *composition* satisfying three properties:

1. (*identity*) There is an element $1 \in G$ such that $1 \circ g = g \circ 1 = g$ for all $g \in G$,
2. (*associativity*) $(g_1 \circ g_2) \circ g_3 = g_1 \circ (g_2 \circ g_3)$ for all $g_1, g_2, g_3 \in G$,
3. (*inverses*) If $g \in G$, then there is an element $g^{-1} \in G$ such that $g \circ g^{-1} = g^{-1} \circ g = 1$.

Definition 4 (Lie group). A group G is a *Lie group* if it is also a smooth manifold over \mathbb{R} and the composition and inversion maps are *smooth*, i.e. infinitely differentiable.

Definition 5 (action). A group G acts on a set S if there is an action map $\cdot: G \times S \rightarrow S$ satisfying

1. $1 \cdot x = x$ for all $x \in S, g \in G$,
2. $g_1 \cdot (g_2 \cdot x) = (g_1 \circ g_2) \cdot x$ for all $x \in S, g_1, g_2 \in G$.

Definition 6 (representation). We say S is a G -*representation* if S is a \mathbb{R} -vector space and G acts on S by linear transformations, that is,

1. $g \cdot (x + y) = g \cdot x + g \cdot y$ for all $x, y \in S, g \in G$,
2. $g \cdot (cx) = c(g \cdot x)$ for all $x \in S, g \in G, c \in \mathbb{R}$.

Definition 7 (direct sum, tensor product). Let V and W be G -representations.

1. The *direct sum* $V \oplus W$ has underlying set $V \times W$. As a vector space it has scalars $c(v, w) = (cv, cw)$ and addition $(v_1, w_1) + (v_2, w_2) = (v_1 + v_2, w_1 + w_2)$. It is a G -representation with action $g \cdot (v, w) = (gv, gw)$.
2. The *tensor product*

$$V \otimes W = \left\{ \sum_i v_i \otimes w_i : v_i \in V, w_i \in W \right\}$$

is a G -representation with action $g \cdot v \otimes w = (gv) \otimes (gw)$.

Definition 8 (irreducible). Let V be a G -representation.

1. If W is a subspace of V and is closed under the action of G , i.e. $gw \in W$ for all $w \in W, g \in G$, then we say it is a *subrepresentation*.
2. If 0 and V itself are the only subrepresentations of V , then it is *irreducible*.

A.2. Decomposition of \mathcal{F}_{ρ_1} into Irreducibles.

We justify the statement that after discretizing and bounding space, i.e. replacing \mathbb{R}^2 by $[0, 64]^2$, and approximating $SO(2)$ by C_n , the space \mathcal{F}_{ρ_1} becomes finite-dimensional and we may decompose $\mathcal{F}_{\rho_1} \cong V^m$ where V is the regular representation.

We can decompose $\mathcal{F}_{\rho_1} \cong \mathcal{F}_{\mathbb{R}} \otimes \rho_1$, i.e. functions on X times the representation ρ_1 . As an $SO(2)$ -representation, $\mathcal{F}_{\mathbb{R}}$ can be further be decomposed by radius since functions on the circle of radius r is a subrepresentation. The space of functions on the circle is isomorphic to the regular representation of $SO(2)$. Thus we have

$$\mathcal{F}_{\rho_1} \cong \left(\bigoplus_r SO(2) \right) \otimes \rho_1 \quad (7)$$

This representation is infinite-dimensional, which is impractical. At this point we discretize. We replace $SO(2)$ by C_n for sufficiently large n and sum over finitely many radii $r = 1, \dots, m$. Thus (7) becomes $V^m \otimes \rho_1$.

A.3. Results on Uniform Motion Equivariance

In this section, we prove that for the combined convolution-activation layers of a CNN to be uniform motion equivariant, the CNN must be an affine function.

Proposition 5. Let $f(\mathbf{X}) = \mathbf{X} * K$ be a convolutional layer with kernel K which is equivariant with respect to arbitrary uniform motion. Then the sum of the weights of K is 1.

Proof. Since f is equivariant, $\mathbf{X} * K + \mathbf{C} = (\mathbf{X} + \mathbf{C}) * K$. By linearity, $\mathbf{C} * K = \mathbf{C}$. Then because \mathbf{C} is a constant vector field, $\mathbf{C} * K = \mathbf{C}(\sum_v K(v))$. As \mathbf{C} is arbitrary, $\sum_v K(v) = 1$. \square

For an activation function to be uniform motion equivariant, it must be a translation.

Proposition 6. Let $\sigma: \mathbb{R} \rightarrow \mathbb{R}$ be a function satisfying $\sigma(x + c) = \sigma(x) + c$. Then σ is a translation.

Proof. Let $a = \sigma(0)$. Then $\sigma(x) = \sigma(x + c) - c$. Choosing $c = -x$ gives $\sigma(x) = a + x$. \square

Proposition 7. Let f be a convolutional layer with kernel K and σ an activation function. Assume σ is piecewise differentiable. Then if the composition $\varphi = \sigma \circ f$ is equivariant with respect to arbitrary uniform motions, it is an affine map of the form $\varphi(\mathbf{X}) = K' * \mathbf{X} + b$, where b is a real number and $\sum_v K'(v) = 1$.

Proof. If f is non-zero, then we can choose x and c and p such that $\alpha = (f(x) + f(c))_p$ and $\beta = (f(x))_p$ are any two

real numbers. Let $\lambda = \sum_v K(v)$. As before $f(c) = \lambda c$. Equivariance thus implies

$$\sigma(\beta + c\lambda) = \sigma(\beta) + c.$$

Let $h = c\lambda$. Then

$$\frac{\sigma(\beta + h) - \sigma(\beta)}{h} = \frac{1}{\lambda}.$$

This holds for arbitrary β and h , and thus we find σ is everywhere differentiable with slope λ^{-1} . So $\sigma(x) = x/\lambda + b$. We can then rescale the convolution kernel $K' = K/\lambda$ to get $\varphi(\mathbf{X}) = K' * \mathbf{X} + b$. \square

Corollary 8. *If f is a CNN alternating between convolutions f_i and activations σ_i and the combined layers $\sigma_i \circ f_i$ are uniform motion equivariant, then f is affine.*

Proof. This follows from Proposition 6 and the fact that composition of affine functions is affine. \square

A.4. Skip Connections and Translation Equivariance

Proposition 9. *Adding skip connections to a translation-equivariant NN preserves translation-equivariance.*

Proof. We denote translation by \mathbf{c} by $\tau(\mathbf{v}) = \mathbf{v} - \mathbf{c}$. Then for $\mathbf{X} \in \mathcal{F}_d$, the translation action $T = T_{\mathbf{c}}^{\text{sp}}$ on fields is just precomposition $T(\mathbf{X}) = \mathbf{X} \circ \tau$. Let $\mathbf{Y} = f(\mathbf{X}) + \mathbf{X}$ be a skip connection where f is translation equivariant and $\mathbf{X}, \mathbf{Y} \in \mathcal{F}_d$. Then we compute

$$\begin{aligned} f(T(\mathbf{X})) + T(\mathbf{X}) &= T(f(\mathbf{X})) + T(\mathbf{X}) \\ &= f(\mathbf{X}) \circ \tau + \mathbf{X} \circ \tau \\ &= (f(\mathbf{X}) + \mathbf{X}) \circ \tau \\ &= \mathbf{Y} \circ \tau \\ &= T(\mathbf{Y}). \end{aligned}$$

as desired. \square

A.5. Results on Scale Equivariance

We show that a scale-invariant CNN in the sense of (2) would be extremely limited. Let $G = (\mathbb{R}_{>0}, \cdot)$ be the rescaling group. It is isomorphic to $(\mathbb{R}, +)$. For c a real number, $\rho_c(\lambda) = \lambda^c$ gives an action of G on \mathbb{R} . There is also, e.g., a two-dimensional representation

$$\rho(\lambda) = \begin{pmatrix} 1 & \log(\lambda) \\ 0 & 1 \end{pmatrix}.$$

Proposition 10. *Let K be a G -equivariant kernel for a convolutional layer. Assume G acts on the input layer by ρ_{in} and output layer by ρ_{out} . Assume that the input layer is padded with 0s. Then K is 1×1 .*

Proof. If $v \neq 0$ then there exists $\lambda \in \mathbb{R}_{>0}$ such that λv is outside the radius of the kernel. So $K(\lambda v) = 0$. Thus by equivariance

$$K(v) = \rho_{out}^{-1}(\lambda)K(\lambda v)\rho_{in}(\lambda) = 0$$

\square

A.6. Equivariance Error.

In practice it is difficult to implement a model which is perfectly equivariant. This results in equivariance error $\text{EE}_T(x) = |T(f(x)) - f(T(x))|$. Given an input x with true output \hat{y} and transformed data $T(x)$, the transformed test error $\text{TTE} = |T(\hat{y}) - f(T(x))|$ can be bounded using the untransformed test error $\text{TE} = |\hat{y} - f(x)|$ and EE .

Proposition 11. *The transformed test error is bounded*

$$\text{TTE} \leq \text{TE} + |T|\text{EE}. \quad (8)$$

Proof. By the triangle inequality

$$\begin{aligned} |T(\hat{y}) - f(T(x))| &\leq |T(\hat{y}) - T(f(x))| + \\ &\quad |T(f(x)) - f(T(x))| \\ &= |T| |\hat{y} - f(x)| + \text{EE}. \end{aligned}$$

\square

A.7. Full Lists of Symmetries of Heat and NS Equations.

Symmetries of NS Equations. The Navier-Stokes equations are invariant under five different transformations (see e.g. (Olver, 2000)),

- Space translation: $T_{\mathbf{v}}^{\text{sp}} \mathbf{w}(\mathbf{x}, t) = \mathbf{w}(\mathbf{x} - \mathbf{v}, t)$, $\mathbf{v} \in \mathbb{R}^2$,
- Time translation: $T_{\tau}^{\text{time}} \mathbf{w}(\mathbf{x}, t) = \mathbf{w}(\mathbf{x}, t - \tau)$, $\tau \in \mathbb{R}$,
- Uniform motion: $T_{\mathbf{c}}^{\text{Gal}} \mathbf{w}(\mathbf{x}, t) = \mathbf{w}(\mathbf{x}, t) + \mathbf{c}$, $\mathbf{c} \in \mathbb{R}^2$,
- Reflect/rotation: $T_R^{\text{rot}} \mathbf{w}(\mathbf{x}, t) = R\mathbf{w}(R^{-1}\mathbf{x}, t)$, $R \in O(2)$,
- Scaling: $T_{\lambda}^{\text{sc}} \mathbf{w}(\mathbf{x}, t) = \lambda \mathbf{w}(\lambda \mathbf{x}, \lambda^2 t)$, $\lambda \in \mathbb{R}_{>0}$.

Individually each of these types of transformations generates a group of symmetries of the system. Collectively, they form a 7-dimensional symmetry group.

Symmetries of Heat Equation. The heat equation has an even larger symmetry group than the NS equations (Olver, 2000). Let $H(\mathbf{x}, t)$ be a solution to $(\mathcal{D}_{\text{heat}})$. Then the following are also solutions:

- Space translation: $H(\mathbf{x} - \mathbf{v}, t)$, $\mathbf{v} \in \mathbb{R}^2$,
- Time translation: $H(\mathbf{x}, t - c)$, $c \in \mathbb{R}$,

- Galilean: $e^{-\mathbf{v} \cdot \mathbf{x} + \mathbf{v} \cdot \mathbf{v} t} H(\mathbf{x} - 2\mathbf{v}t, t)$, $\mathbf{v} \in \mathbb{R}^2$
- Reflect/Rotation: $H(R\mathbf{x}, t)$, $R \in O(2)$,
- Scaling: $H(\lambda\mathbf{x}, \lambda^2 t)$, $\lambda \in \mathbb{R}_{>0}$
- Linearity: $\lambda H(\mathbf{x}, t)$, $\lambda \in \mathbb{R}$ and $H(\mathbf{x}, t) + H_1(\mathbf{x}, t)$,
 $H_1 \in \text{Sol}(\mathcal{D}_{\text{heat}})$
- Inversion: $a(t)e^{-a(t)c\mathbf{x} \cdot \mathbf{x}} H(a(t)\mathbf{x}, a(t)t)$, where
 $a(t) = (1 + 4ct)^{-1}$, $c \in \mathbb{R}$.

A.8. Additional Details on Training and Hyper-parameters

Table 4 compares the number of parameters used in each of our models. Table 5 gives the hyper-parameter tuning range for our models.

Table 4. The number of parameters in each model, the time costs for training an epoch on 8 V 100 GPUs.

ResNet	<i>Reg</i>	<i>UM</i>	<i>Mag</i>	<i>Rot</i>	<i>Scale</i>	U-net	<i>Reg</i>	<i>UM</i>	<i>Mag</i>	<i>Rot</i>	<i>Scale</i>
<i>#Params</i> (10^6)	11.03	11.03	11.03	10.16	10.70		6.24	6.24	6.24	7.11	5.99
<i>Time</i> (<i>min</i>)	3.04	5.21	5.50	14.31	160.32		2.15	4.32	4.81	11.32	135.72

Table 5. The Hyper-parameter tuning range. Learning rate, the number of accumulated errors for backpropogation, the number of input frames, batch size, and the hidden dimension and the number of layers for CNNs

<i>Learning rate</i>	<i>#Accumulated Errors</i>	<i>#Input frames</i>	<i>Batch Size</i>	<i>Hidden Dim (CNNs)</i>	<i>#Layers (CNNs)</i>
1e-1 ~ 1e-6	1~10	1~40	4~64	8~128	1~10